

# A rapid and versatile method for solvothermal synthesis of $\text{Sb}_2\text{O}_3$ nanocrystals under mild conditions

K. Kaviyarasu · D. Sajan · Prem Anand Devarajan

Received: 17 July 2012 / Accepted: 1 September 2012 / Published online: 18 September 2012  
© The Author(s) 2012. This article is published with open access at Springerlink.com

**Abstract** A very simple strategy for preparing  $\text{Sb}_2\text{O}_3$  nanostructures under ambient aqueous condition is presented.  $\text{Sb}_2\text{O}_3$  nanoparticles with an average size of approximately 44 nm were synthesised using wet chemical method. Senarmonite cubical structure  $\text{Sb}_2\text{O}_3$  nanocrystals have been selectively harvested in high yield. The as-obtained nanoproducs were characterized by X-ray powder diffraction, Fourier transform infrared (FTIR), ultraviolet–visible near infrared spectroscopy (UV–Vis–NIR) and scanning electron microscopy (SEM) analyses. The size of the  $\text{Sb}_2\text{O}_3$  nanoparticles was found to be in the range 44–385 nm from Debye–Scherrer equation. The X-ray density, surface area and porosity of  $\text{Sb}_2\text{O}_3$  nanocrystals were found to be  $2.969 \text{ g/cm}^3$ ,  $2.0208 \times 10^{14} \text{ cm}^2/\text{g}$  and  $1.0185 \times 10^{-3} \text{ m}$ , respectively. From the UV–Vis–NIR analysis, the band gap of  $\text{Sb}_2\text{O}_3$  nanocrystals was estimated to be 5.6 eV at 220 nm. The various functional groups in the samples were identified using FTIR spectral studies. The SEM images showed a very spiky morphology. Very small spherical-shaped objects were clearly observed within these structures. The extinction coefficient, real and imaginary part of the dielectric constant, electric susceptibility and the refractive index of  $\text{Sb}_2\text{O}_3$  nanocrystals were  $7.605 \times 10^{-9}$ ,  $0.2851 \times 10^{-17}$ ,  $3.747 \times 10^{-8}$ , 0.48322 and 2.4636, respectively.

**Keywords** Antimony trioxide ( $\text{Sb}_2\text{O}_3$ ) · PEG-6000 · X-ray powder diffraction (XRPD) · Ultraviolet–visible analysis (UV–Vis–NIR) · Fourier transform infrared analysis (FTIR) · Scanning electron microscopy (SEM)

## Introduction

It is now wide accepted that many fundamental properties of nanocrystals depend strongly on their shape, size and microstructure. Over the past decades, driven by the development of next generation low cost nano devices, researchers have been exploring ways to control shapes of nano building blocks. Recently, oxide nanoparticles have increasingly gaining interest over past decade to the possibilities of fabricating the nanostructured materials showing novel properties compared with bulk materials (Linderth and Pedersen 1994; Iwanaga et al. 1998). Antimony trioxide ( $\text{Sb}_2\text{O}_3$ ) is regarded as one of the important sensor materials for detecting leakage of inflammable gases because of their high sensitivity to low gas concentration (Yamazoe 1991) and wide industrial such as conductive material, functional filters, adhesives and textile back coating (Sato et al. 1998). In addition,  $\text{Sb}_2\text{O}_3$  is used as a catalyst in the polyester industry and as a clarifying agent in optical glass, television tubes crystal production and in dielectric coatings (Chin et al. 2007; Liu and Iwasawa 2002; Lewis and Jordan 1970; Jenkins 1958; Honica and Krebs 1959). Upto now, utilising different synthesis, a great number of nanomaterials such as  $\text{ZnO}$ ,  $\text{TiO}_2$ ,  $\text{Co}_3\text{O}_4$  and  $\text{V}_2\text{O}_5$  have been successfully obtained (Guo and Liu 2007; Nakajima et al. 2000; Lim et al. 2007; Li et al. 2001; Joseph et al. 2006; Gao and McGarthy 2006; Feng et al. 2005; Wang et al. 2006). To the best of our knowledge, only a limited number of articles pertaining to

K. Kaviyarasu · P. A. Devarajan (✉)  
Department of Physics, St. Xavier's College,  
Palayamkottai 627 002, India  
e-mail: dpremanand@yahoo.co.in

D. Sajan  
Department of Physics, Bishop Moore College,  
Mavelikara, Kerala 690 110, India

TEM, AFM, and FESEM of  $\text{Sb}_2\text{O}_3$  nanocrystals have been published (Liu et al. 2004; Zhu et al. 2006; Feng et al. 2004; Wood et al. 1972; Wolfing and Hurrych 1973). In this paper, we present the fabrication of nanocrystals. Further more in our case, the as-synthesized  $\text{Sb}_2\text{O}_3$  nanocrystals exist relating to a smaller particle size obtained by one step solvothermal synthesis and these crystals are characterized by XRPD, FTIR, UV–Vis-NIR and SEM analyses.

## Experimental procedure

### Materials

Antimony trioxide ( $\text{Sb}_2\text{O}_3$ ), ethanol ( $\text{C}_2\text{H}_5\text{OH}$ ) and PEG-6000 were purchased from E-Merck. All the reagents used in the experiments were analytical grade and used without further purification. Double deionised distilled water was used throughout the experiment.

### Synthesis of $\text{Sb}_2\text{O}_3$ nanocrystals

In a typical process, 0.1 M of  $\text{Sb}_2\text{O}_3$  was dissolved in 40 ml of ethanol with vigorous stirring to form a homogeneous solution. 50 mg of PEG-6000 was added to the above solution under continuous stirring until an opalescent mixture was obtained. Then the mixture was stirred for another 30 min, and about 15 ml of mixture was transferred into a Teflon-lined stainless steel autoclave 60 ml of 70 % capacity of the total volume. The autoclave was hermitically sealed and maintained at 120 °C for 12 h, and then cooled to room temperature normally. The resultant white precipitate was centrifuged, washed several times with distilled water and  $\text{CCl}_4$  was added to remove the impurities and then dried at 60 °C for 3 h. The white product so processed was later used for different characterization studies.

### Characterization techniques

X-ray powder diffraction (XRPD) of the products was measured using a *D/max* (2,500 V, Rigaku, JAPAN) and X-ray powder diffractometer at a scanning rate  $2\theta$  ranging from 10° to 70° using  $\text{CuK}_\alpha$  radiation ( $\lambda = 0.15418$  nm). For the optical absorption studies, UV–Vis-NIR (Hitachi U-3400) spectrophotometer was used. Fourier transform infrared spectroscopy (FTIR) spectra were recorded with a Nicolet Avatar-370 spectrometer equipped with a TGS/PE detector and a silicon beam splitter with  $1\text{ cm}^{-1}$  resolution. The sizes and morphologies of the products were investigated by a scanning electron microscopy (SEM), performed on a JSM-6700F at an acceleration voltage of 16.0 kV scanning electron microanalyses.

## Results and discussion

### X-ray powder diffraction analysis

Figure 1 presents the XRPD patterned as-synthesised  $\text{Sb}_2\text{O}_3$  nanoparticles. From XRPD diffractogram, all labelled reflection peaks can be readily indexed to the senarmontite structure as per the standard ASTM card. No evidence of metallic antimony signal was detected in the nanosamples. In addition, no obvious impurities could be detected in the pattern, and the sharp strong characteristic peaks suggest that the resulting products were well crystallized. The size of the  $\text{Sb}_2\text{O}_3$  nanoparticles were determined by applying the Debye–Scherrer equation to the half intensity width of the (111), (121) and (012) peaks. The average size of the nanocrystallites was also estimated using Debye–Scherrer formula:

$$d = 0.9\lambda / \beta \cos \theta \quad (1)$$

where  $\lambda$ ,  $\beta$  and  $\theta$  are the X-ray wavelength, the full width at half maximum (FWHM) of the diffraction peak and the Bragg diffraction angle, respectively. The estimated crystalline size was found to vary from 44 to 385 nm from XRPD data. It is known that for cubical structure, the lattice parameter can be calculated by the formula:

$$d_{hkl} = a / \sqrt{h^2 + k^2 + l^2} \quad (2)$$

where  $h$ ,  $k$ , and  $l$  are all integers,  $(hkl)$  in the lattice place index and  $a$  in the lattice constant. The strongest peak (111) was used to estimate the lattice expansion of the nanocrystals. The lattice parameter was estimated to be 2.3538 Å. The X-ray density for a cubical system is evaluated using the formula:

$$D_x = 8M / Na^3 \quad (3)$$

where  $M$  is the molecular weight,  $N$  is the Avogadro number and  $a$  is the lattice constant.

The density was found to be  $D_x = 2.96919\text{ g/cm}^3$ . Further, the specific area of the  $\text{Sb}_2\text{O}_3$  nanoflakes along the strongest peak is calculated using the formula:

$$S_a = 6 / DD_x \quad (4)$$

where  $D$  and  $D_x$  are the particle size and X-ray density of the  $\text{Sb}_2\text{O}_3$  nanocrystals, respectively. The specific area of  $\text{Sb}_2\text{O}_3$  nanocrystal was found to be  $2.020814 \times 10^4\text{ cm}^2/\text{g}$ .

### Ultraviolet–visible-NIR absorption studies

The band gap of the bulk  $\text{Sb}_2\text{O}_3$  crystal is 3.30 eV, which was determined by the UV–Vis-NIR transmission spectrum in the 1970's (Ashour et al. 1995; Kaid and Ashour 2007; Gupta and Mansingh 1996). Here, an optical absorption study is carried out in order to provide a simple and an

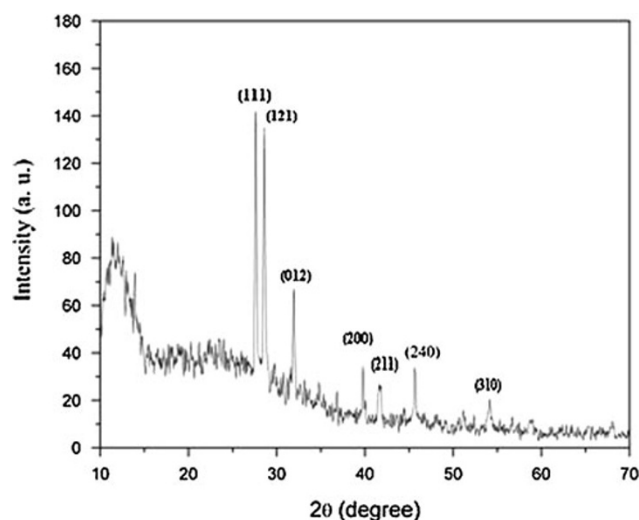


**Fig. 1** XRPD pattern of  $\text{Sb}_2\text{O}_3$  nanocrystals

effective method to explain some features concerning the optical band gap structure. Figure 2 shows the UV–Vis–NIR absorption spectrum of spherical  $\text{Sb}_2\text{O}_3$  nanoparticles measured at room temperature in the wavelength ranging from 190 to 1,100 nm. The spectrum shows that band with a prominent absorption, maximum at 220 nm, was attributed to the band gap absorption appearing in the visible region. The optical band gap ( $E_g$ ) was evaluated from the transmission spectra and the optical absorption coefficient ( $\alpha$ ) near the absorption edge is given by (Chin et al. 2007):

$$h\nu = A(h\nu - E_g)^{1/2} \quad (5)$$

where  $A$  is constant,  $E_g$  in the optical band gap,  $h$  is the Planck's constant and  $\nu$  is the frequency of the incident photons. The band gap of the  $\text{Sb}_2\text{O}_3$  nanocrystal was estimated by plotting  $(\alpha h\nu)^{1/2}$  versus  $h\nu$  and extrapolating the linear portion near the onset of absorption edge to the energy axis. The value of band gap is 3.3 eV. The measured transmittance ( $T$ ) was used to calculate the absorption coefficient ( $\alpha$ ) using the formula:

$$\alpha = \frac{2.3026 \log(1/T)}{t} \quad (6)$$

where  $t$  is the diameter size of the nanosample. The extinction coefficient ( $\alpha$ ) is got from the following relation:

$$K = \frac{\lambda \alpha}{4\pi} \quad (7)$$

The transmittance ( $T$ ) is given by,

$$T = \frac{1 - R^2 \exp(-\alpha t)}{1 - R^2 \exp(-2\alpha t)} \quad (8)$$

which is constant at  $\lambda = 220$  nm. The reflectance ( $R$ ) in terms of the absorption coefficient is found using the following equation

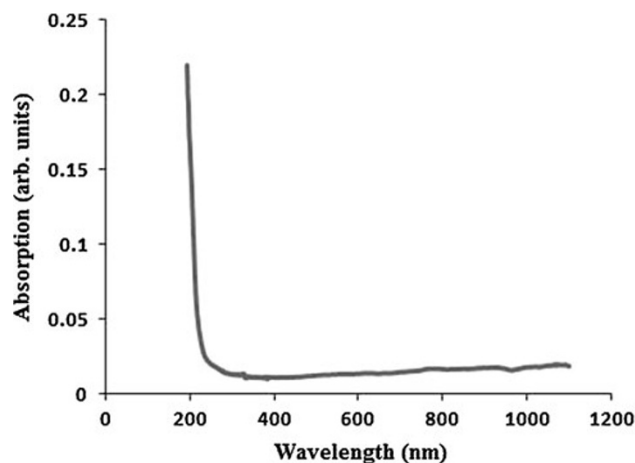


**Fig. 2** UV-Vis-NIR absorption spectrum of  $\text{Sb}_2\text{O}_3$  nanocrystals

$$R = \frac{\exp(-\alpha t) \pm \sqrt{\exp(-\alpha t)T - \sqrt{\exp(-3\alpha t)T + \exp(-2\alpha t)T^2}}}{\exp(-\alpha t) + \exp(-2\alpha t)T} \quad (9)$$

The refractive index ( $n$ ) is calculated using,

$$n = \frac{-(R + 1) \pm 2\sqrt{R}}{(R - 1)} \quad (10)$$

The refractive index  $n$  is 2.4636 for  $\text{Sb}_2\text{O}_3$  nanocrystallites. From the optical constants, the electrical susceptibility ( $\chi_c$ ) is calculated using the equation,

$$\epsilon_r = \epsilon_0 + 4\pi\chi_c = n^2 - k^2 \quad (11)$$

$$\chi_c = \frac{n^2 - k^2 - \epsilon_0}{4\pi} \quad (12)$$

where  $\epsilon_0$  is the dielectric constant in the absence of any contribution from free carriers. The value of electric susceptibility ( $\chi_c$ ) is 0.48322 at  $\lambda = 220$  nm. The real part dielectric constant ( $\epsilon_r$ ) and imaginary part of dielectric constant ( $\epsilon_i$ ) is calculated using the following equation:

$$\epsilon_r = n^2 - k^2 \quad (13)$$

$$\epsilon_i = 2nk \quad (14)$$

The values of real ( $\epsilon_r$ ) and imaginary ( $\epsilon_i$ ) dielectric constant were found to be  $\epsilon_r = 0.2851 \times 10^{-17}$  and  $\epsilon_i = 3.747 \times 10^{-8}$ .

#### Fourier transform infrared spectrum

FTIR spectra of  $\text{Sb}_2\text{O}_3$  nanocrystal were carried out in the middle IR region between the wave number 400 and 4,000  $\text{cm}^{-1}$ . The spectra obtained are shown in Fig. 3. The peaks at 3,727.28 and 3,122.67 are attributed to two water bands corresponding to stretching and bending vibration. These regions indicate the hydroscopic character of the powder samples. The peaks at 733 and 601.07 are assigned

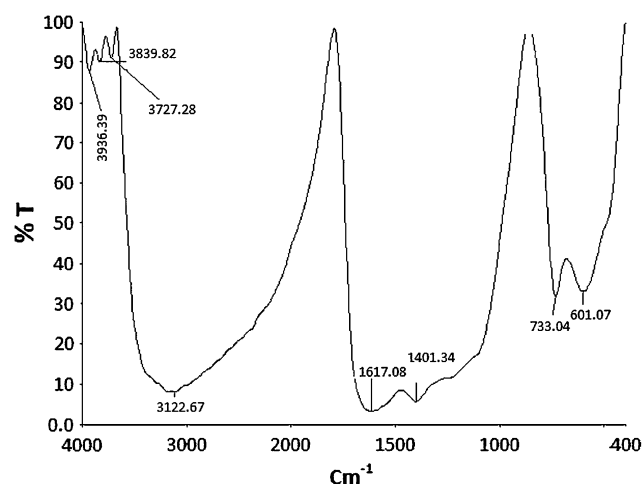


**Fig. 3** FTIR spectrum of  $\text{Sb}_2\text{O}_3$  nanocrystals

to the Sb–O–Sb vibrations. The small absorption due to metal oxygen (N–O) stretching is also seen at around  $601\text{ cm}^{-1}$ . The spectra of this sample heated at  $120^\circ\text{C}$  show the sharpening of the bands and slight shift to the higher frequency have been observed. This exhibits occurrence of the band shortening and reduction in the mean Sb–O–Sb in the bond angle (Gaffar et al. 2003; Bosshard et al. 1993; Hatton et al. 2006; Austin and Mott 1969; Benet and Gnanam 1994).

#### Scanning electron microscope analysis

The morphologies of the resulting products were examined using SEM. Figure 4 exhibits SEM images of the prepared  $\text{Sb}_2\text{O}_3$  sample. It is well established that the majority of the nanocrystallite have spherical shape with a diameter of about  $44\text{ nm}$  at the centre and length  $385\text{ nm}$  on average, which is similar to the quasi-spherical  $\text{Sb}_2\text{O}_3$  nanoparticles produced by the  $\gamma$ -ray radiation oxidation route (Dzimitrowice et al. 1982).

#### Conclusion

A very simple and convenient method was adapted to grown  $\text{Sb}_2\text{O}_3$  nanocrystal by wet chemical method. The perfection of crystallinity was confirmed XRPD and the peaks were indexed. The band gap and the related physical parameters were evaluated using UV–Vis–NIR analysis. The various functional groups in the molecule were elucidated by FTIR spectral analysis. The size of the as-obtained  $\text{Sb}_2\text{O}_3$  nanocrystals were predicted using SEM topography and the results are in good agreement with the XRPD results. FESEM, AFM and PL studies are in progress.

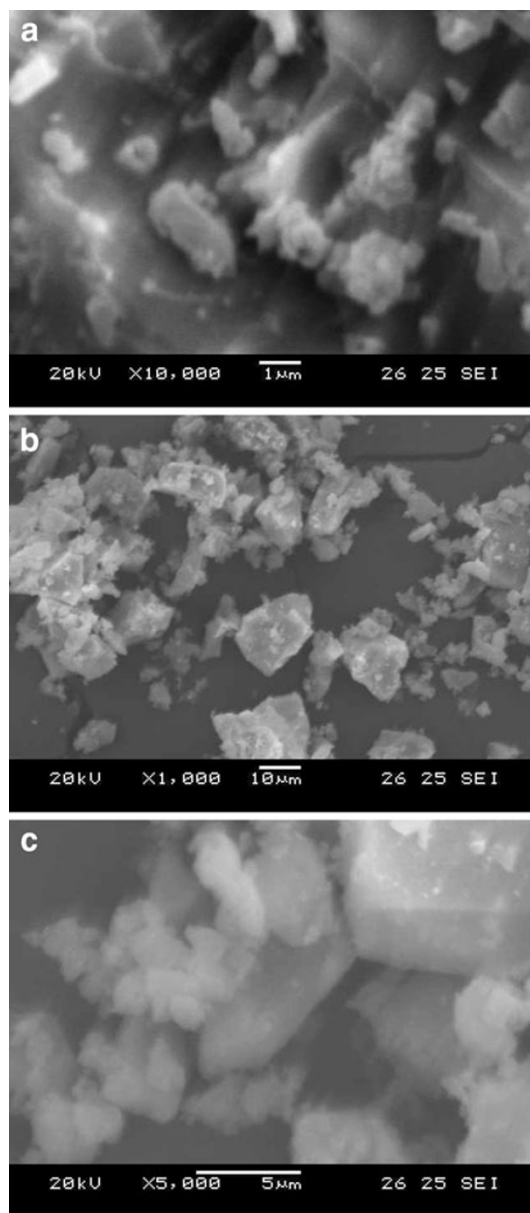


**Fig. 4** SEM images of  $\text{Sb}_2\text{O}_3$  nanocrystals

**Acknowledgments** One of the authors (K. Kaviyarasu) would like to thank Dr. S. Paulraj, Head of the Department of Physics, St. Xavier's College, Palayamkottai for his constant support, help and encouragement.

**Open Access** This article is distributed under the terms of the Creative Commons Attribution License which permits any use, distribution, and reproduction in any medium, provided the original author(s) and the source are credited.

#### References

- Ashour A, El-kadry N, Mahmoud SA (1995) Physical properties of spray pyrolysed CdS thin films. *Thin Solid Films* 26:117

- Austin IG, Mott NF (1969) Band structure of magnetic semiconductors. *Adv Phys* 18:41
- Bosshard CH, Sutter K, Schlessner R, Gunter R (1993) Influence of strontium doping on the indirect band gap and optical constants of ammonium zinc chloride crystals. *Opt Soc Am B* 10:867
- Chin HS, Cheong KY, Brebua M, Jakabb E, Sakataa Y (2010) Review on oxides of antimony nanoparticles: synthesis, properties, and applications. *J Mater Sci* 45:5993
- Dzimitrowice DJ, Good enough BJ, Wiseman PJ (1982) Characteristics of  $\text{Sb}_2\text{O}_3$  nanoparticles synthesized from antimony by vapor condensation method. *Mater Res Bull* 17:971
- Feng XJ, Feng L, Jin MH, Zhai J, Jiang L, Zhu BD (2004) Progress in superhydrophobic surface development. *J Am Chem Soc* 126:62
- Feng XF, Zhai J, Jiang L (2005) The fabrication and switchable superhydrophobicity of  $\text{TiO}_2$  nanorod films. *Angew Chem* 44:5115
- Gaffar MA, AbuEl-Fadl A, Bin Anooz S (2003) Growth, optical, mechanical and dielectric properties of glycine zinc chloride NLO crystals. *Phys B* 327:43
- Gao LC, McGarthy TJ (2006) A general approach for fabrication of super hydrophobic and superamphiphobic surfaces. *J Am Chem Soc* 128:9052
- Gnanam FD (1994) Synthesis, crystal growth and characterization of novel semiorganic nonlinear optical crystal: dichlorobis(1-proline)zinc(II). *Cryst Res Technol* 29:707
- Guo ZG, Liu WM (2007) Superhydrophobic spiral  $\text{Co}_3\text{O}_4$  nanorod arrays. *Appl Phys Lett* 90:193108
- Gupta V, Mansingh A (1996) Temperature dependent optical properties of (002) oriented ZnO thin film using surface plasmon resonance. *J Appl Phys* 80:1063
- Hatton BD, Landskron K, Hunks WJ, Bennett MR (2006) Dielectric materials research for advanced microelectronic devices. *Mater Today* 9:22
- Honica G, Krebs K (1959) Interference filters for the far ultraviolet (1,700 Å to 2,400 Å). *Physik* 156:117
- Iwanaga H, Fujii M, Takeuchi S (1993) Growth model of tetrapod zinc oxide particles. *J Crys Grow* 134:275
- Jenkins FA (1985) Multilayer reflection coatings on a metal mirror. *J Phys Radium* 19:301
- Joseph P, Cottin-Bizonne C, Benoit JM, Ybert C, Journet C, Tabeling P (2006) Anisotropic flow in striped superhydrophobic channels. *Phys Rev Lett* 97:156104
- Kaid MA, Ashour A (2007) Sol-gel preparation, characterization and electrical properties of nanosized gallium doped zinc-oxide. *Appl Surf Sci* 253:3029
- Lewis B, Jordan MR (1970) Morphological changes in Se films deposited on KI irradiated by electrons. *Thin Solid Films* 6:289
- Li HJ, Wang HB, Song YL, Liu YQ, Li QS, Jiang L, Zhu DB (2008) Wettability switching between high hydrophilicity at low pH and high hydrophobicity at high pH on surface based on pH-responsive polymer. *Chem Commun* 10:1199
- Lim HS, Kwak D, Lee DY, Lee SG, Cho K (2007) Reversible ultraviolet light-manipulated superhydrophobic-to-superhydrophilic transition on a tubular SiC nanostructure film. *J Am Chem Soc* 129:4128
- Linderorth S, Pedersen MS (1994) Fe- $\text{Al}_2\text{O}_3$  nanocomposites prepared by high energy ball milling. *J Appl Phys* 75:5867
- Liu H, Iwasawa Y (2002) Synthesis and purple-blue emission of antimony trioxide single-crystalline nanobelts with elliptical cross section. *J Phys Chem B* 106:2319
- Liu H, Feng L, Zhai J, Jiang L, Zhu B (2010) Nanometric multiscale rough Zn-ZnO superhydrophobic thin films: Self-diffusion of zinc and effect of UV irradiation. *Appl Phys Lett* 97:183112
- Nakajima A, Hashimoto K, Watanabe T, Takai K, Yamauchi G, Fujishima A (2005) pH-dependent structure and properties of  $\text{TiO}_2/\text{SiO}_2$  nanoparticle multilayer thin films. *Langmuir* 16:7044
- Sato H, Kondo K, Tsuge S, Ohtani H, Sato N (1998) Flame retardant mechanism of polydimethylsiloxane material containing platinum compound studied by analytical pyrolysis techniques and alkaline hydrolysis gas chromatography. *Polym Degrad Stab* 62:41
- Wang ST, Feng XJ, Yao JN, Jiang L (2010) Reversible ultraviolet light-manipulated superhydrophobic-to-superhydrophilic transition on a tubular SiC nanostructure film. *Appl Phys Lett* 97:183112
- Wolfing B, Hurych Z (1973) Atomically clean surfaces of elemental solids. *J Phys Status solids A* 16:161
- Wood C, Van Pelt B, Dwight A (1972) Controllable synthesis and formation mechanism of bow-tie-like  $\text{Sb}_2\text{O}_3$ . *J Phys Status solids B* 54:701
- Yamazoe N et al (1991) New approaches for improving semiconductor gas sensors. *Sens Actuators B* 5:7
- Zhu WQ, Feng XJ, Feng L, Jiang L (2010) Reversible ultraviolet light-manipulated superhydrophobic-to-superhydrophilic transition on a tubular SiC nanostructure film. *Appl Phys Lett* 97:183112